Modeling, Analysis, and Mitigation of Active Power Oscillation in Parallel VSGs System

Jiadong Sun, Xiangyang Xing, *Member, IEEE*, and Chenghui Zhang, *Fellow, IEEE*

***Abstract*—Recent years, the virtual synchronous generator (VSG) is widely used in practice, owing to its ability to emulate the behavior of traditional synchronous generators. However, a challenge issue emerges during load changes, namely, the active power oscillation tends to cause overload and frequency stability deterioration, especially in the parallel VSGs system. Although some studies have tried to address this issue, the effectiveness of conventional methods based on small signal model (model linearization) are influenced by the change of equilibrium point. And the linear method of parallel VSGs system is lack of a stable design framework. As the number of VSGs increases, the order of model will increase rapidly, then the stability of parallel system is difficult to be proven by the root locus or other linear stability criteria. Therefore, in this article, the port-controlled Hamiltonian model is first built, which provides a stable framework for control law designing. Then, this model is employed to investigate the impact of coupling effect between parallel VSGs, which induces the oscillation. Furthermore, to mitigate the active power oscillation and enhance the frequency stability, the coupling effect is regarded as the disturbance, and a control law is proposed to constrain the impact of disturbance based on the L_2-disturbance attenuation. Finally, effectiveness of the proposed strategy is validated by simulations and experiments.**

***Index Terms*—Active power oscillation, frequency stability, L2-disturbance attenuation, parallel system, port-controlled Hamiltonian (PCH) system, virtual synchronous generator (VSG).**

I. Introduction

As the penetration rate of distributed generators (DGs) increases, inertia of the power system is declined, inevitably, which threatens the safe and stable operation of this system. To address this problem, virtual synchronous generator (VSG) is employed to play the role of conventional synchronous generators (SGs) in the power system, especially, in the microgrid [1], [2], where the load is widely powered by the distributed generators (DGs) rather than the public power grid. Impacts of VSGs on the power system are studied in many literatures. In [3] and [4], it is pointed out that the frequency stability of the DGs-feed system is improved by VSG. In [5] and [6], in order to analyze the stability of grid-connected system with VSGs, sequence impedance modeling is constructed. In [7], based on the small signal model of VSG, the control parameters of the VSG are designed.

However, due to the mimic of conventional SGs, the output active power oscillation of the VSG will be found when the load fluctuation occurs. Particularly, the load will abruptly change when powered devices are connected into or cut OFF from the ac source composed of the VSGs. Differentiating from the conventional SGs [8], the employment of semiconductor devices makes the VSGs is liable to the overload, which is induced by the active power oscillation when the load abrupt changes. In [9], [10], and [11], the power coupling between the active power loop and the reactive power loop is studied, which conclude that the power coupling can be neglected when the line reactance is much larger than the line resistance. In addition, the dynamic properties of the single VSG system are fully studied. In [12], the VSG control changes to the generalized droop control when the disturbance occurs to achieve a rapid power tracking performance and suppress the active power oscillation. In [13] and [14], the VSG with adaptive inertia and damping is proposed to improve the dynamic performance. In [15], a novel control method is proposed, which enhances the frequency stability by a switched active power control to make the state variables converge to their equilibrium point (EP) along designed phase trajectories. In [16], the passivity-based control (PBC) is employed, which extracts the disturbance active power and the angular frequency of VSG to be state variables of the linear PBC model by employing a washout filter.

In order to improve the reliability and capacity of the system fed by DGs, the parallel VSGs system is widely applied in practice. Due to the virtual inertia, the parallel VSGs attract much attention in supporting the microgrid, which can upgrade the frequency stability and share the load power according to the capacity of each VSG, which are studied by the [17], [18]. However, active power oscillation is also found in the parallel VSGs system when the load changes. In the parallel system, the ac bus frequency is supported by VSGs, the active power oscillation will cause the frequency fluctuation of the ac bus and may induce more severe cascading issues. Additionally, due to the dynamical interactions between parallel VSGs, the mechanism of active power oscillation in parallel VSGs system is much more complex than that in single VSG system. Thus,

Received 22 September 2024; revised 14 January 2025 and 8 May 2025; accepted 4 July 2025. Date of publication 28 July 2025; date of current version 27 August 2025. This work was supported in part by the National Natural Science Foundation of China under Grant 62222309, in part by the Natural Science Foundation of Shandong Province under Grant ZR2022JQ29, and in part by the Major Scientific and Technological Innovation Project of Shandong Province under Grant 2024ZLGX04 and Grant ZFJH202301. Recommended for publication by Associate Editor M. Molinas. *(Corresponding author: Xiangyang Xing.)*

The authors are with the School of Control Science and Engineering, Shandong University, Jinan 250061, China (e-mail: 202214786@mail.sdu.edu.cn; xyxing@sdu.edu.cn; zchui@sdu.edu.cn).

Color versions of one or more figures in this article are available at https://doi.org/10.1109/TPEL.2025.3589731.

Digital Object Identifier 10.1109/TPEL.2025.3589731

the methods mentioned above as [13], [14], [15], [16] are not effective in the parallel VSGs system. In [13] and [14], even the communication is employed, the parameter adjustment is hard to coordinate with the other VSGs, which may induce new oscillations, then the proper coordination method is needed. In [15], the power sharing is not considered when the method is applied in a parallel system. In [16], the estimation or observation of the ac bus frequency and the line impedance is difficult to achieve in the parallel VSGs system. In addition to the mentioned above, the modeling and stability analysis is also much more complex than that of single VSG system, which makes the active power oscillation in the parallel VSGs system to be a new issue.

To address this issue, the active power oscillation in the parallel VSGs system is researched in some literatures as below. In [19], the reason of active power oscillation is analyzed, and the state space equation based on the two parallel VSGs is obtained. In [20], the active power oscillation between two parallel VSGs is mitigated by introducing the virtual reactance. In [21], an adaptive adjustment method of the virtual inertia and the damping is proposed to improve the frequency response. In [22], the self-damping and the mutual damping are designed by an optimization method to mitigate the active power oscillation. In [23], the active power oscillation in the parallel VSGs system composed of *N* VSGs is analyzed based on the aggravated modeling. In [24], a phase feedforward damping control is proposed to mitigate the active power oscillation. In [25], a transient active power sharing strategy based on the small signal modeling is proposed, which enhances the frequency stability by regulating the inertia parameter. In [26], a decentralized mutual damping control is proposed, which employs the output reactive power. In [27], both the damping and the feedback of disturbance in output active power are employed to mitigate the active power oscillation. In [28], the active power oscillation is analyzed in terms of a single VSG by regarding all the influence caused by the load fluctuation as a disturbance to the active power loop.

Nevertheless, the existing methods are supposed to have some drawbacks. In [19] and [20], only two parallel VSGs system is analyzed, and the real time information of line impedance is needed to design the virtual impedance, which is difficult to obtain in practice. In [21], the feasibility in parallel *N* VSGs system is not fully discussed. In [22], the optimization is some complex and multiple iterations required, which may not have enough robustness when the EP of system fluctuations. In [23], the line impedance is also needed and the assumption that no power flow between the similar VSGs is overly ideal. In [24], due to the feedforward of phase angle, it is noted that the proposed method will eliminate the inertia property of VSG. In [26], the proposed strategy is only suitable for the cascaded type connected VSGs. In [27] and [28], the high pass filter in power feedback link for eliminating dominant poles reduces the frequency stability and the ac bus voltage required by [27] is difficult to obtain in practice.

Moreover, the main studies and methods mentioned above are based on the small signal model, where the state space matrix is influenced by the position of EP, which will be affected by the change of load and line impedance. As a result, the robustness of methods that relies on regulating the location of eigenvalues is decreased. Considering this, the parallel *N* VSGs is realized as a port-controlled Hamiltonian (PCH) system to prevent the model from being affected by the EP changing and elaborate the coupling effect between parallel VSGs. Based on this model, the active power oscillation can be represented by the increase of Hamiltonian function and then mitigated by the proposed nonlinear strategy. Furthermore, while the conventional methods above demonstrate stability for two parallel VSGs system, their scalability remains unverified as the number of VSG increases, where system order and complexity grow substantially. The contributions of this article are as follows:

1) To prevent the model from being affected by EP changing (caused by the variation of line impedance and load) and provide a stable framework for control law designing, the PCH model of parallel *N* VSGs system is first built. Based on the PCH model, the issue caused by EP changing in the linearized model is avoided and the stability of parallel system can be guaranteed if only the system structure with the proposed control law satisfies the requirement of interconnection and dissipation.
2) The coupling effect between parallel VSGs is investigated, revealing that it induces oscillations in both active power and angular frequency.
3) Based on the L_2-disturbance attenuation, the impact of coupling effect between parallel VSGs is constrained by the proposed strategy, which simultaneously achieves mitigation on active power oscillation and enhancement on angular frequency while preserving the inertia property. Since the proposed strategy is independent of EP changing, it exhibits superior robustness as the line impedance changes. Moreover, the proposed strategy is communication-free and without the need for line impedance and ac bus information, which reduces the complexity of the parallel system in practice.

The rest of this article is organized as follows. In Section II, the parallel VSGs system is overviewed. In Section III, the PCH model of parallel VSGs system is constructed and the impact of coupling effect between VSGs is analyzed. The proposed strategy is shown in the Section IV. In Section V, the proposed strategy is validated by simulations and experiments. Finally, Section VI concludes this article.

II. Overview of the Active Power Oscillation

A. Overview of the Parallel N VSGs System

The VSG control algorithm is shown in Fig. 1, where the output phase angle θ_m and the output angular frequency ω_m are controlled by the active power loop (APL) and the amplitude of output voltage is controlled by the reactive power loop (RPL). The APL includes the parameters *J*, *D*, which are used to mimic the rotation equation of the traditional SGs. And the RPL contains the parameters K_u, K_q, which introduces the droop control of reactive power.

Besides, the reference active power, the reference reactive power, and the reference output voltage amplitude are represented as P_{ref}, Q_{ref}, and U_{ref}, respectively. Noting that the reference angular frequency, i.e., ω_0 is determined by the power

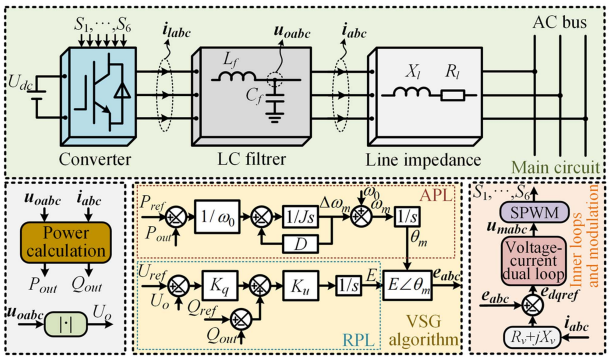

Fig. 1. VSG control algorithm.

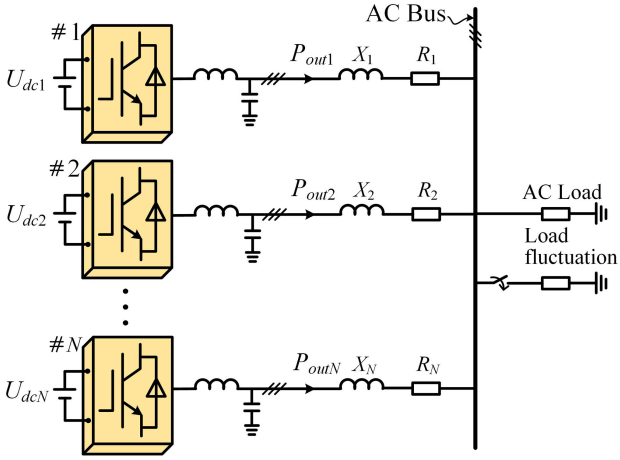

Fig. 2. Overview of the parallel *N* VSGs system.

system, which is 100π in this article, and $\Delta\omega_m$ is the difference between ω_m and ω_0. Main circuit of the single VSG system consists of a dc-source $U_{\rm dc}$, a *LC* filter contains inductor L_f and capacitor C_f, and the line reactance, line resistance denoted as X_l, R_l, respectively. The three phase inductor current is $\boldsymbol{i}_{labc}$, and $\boldsymbol{i}_{abc}$, $\boldsymbol{u}_{oabc}$ represent the three phase output current, the three phase output voltage, respectively. Since the dynamic response of the voltage-current dual loop is much faster than that of power loop, the output voltage $\boldsymbol{u}_{oabc}$ is assumed to be the output voltage of the power loop, i.e., $\boldsymbol{e}_{abc}$, then the amplitude of output voltage $\boldsymbol{u}_{oabc}$ can be regarded as E.

The parallel *N* VSGs system is depicted in Fig. 2, where the variables of the *i*th VSG is represented by a subscript "*i*". In order to simplify the analysis of active power oscillation, by employing the virtual impedance, the line reactance can always be assumed to be much larger than the line resistance [25], then the coupling between APL and RPL can be neglected [10], [11], [25]. Thus, analyzing the active power oscillation can only take the interactions between the APL of parallel VSGs into account. From Fig. 1, the APL of the *i*th VSG can be expressed as

$$\begin{cases} \dot{\delta}_i = \omega_{mi} - \omega_{bus} \\ J_i\omega_0 \cdot \Delta\dot{\omega}_{mi} = P_{refi} - \frac{1.5E_i \cdot U_{bus}}{X_{li}} \sin\delta_i - D_i\omega_0 \cdot \Delta\omega_{mi} \end{cases} \tag{1}$$

where the ω_{bus} and the U_{bus} are the angular frequency and the amplitude of the ac bus voltage, respectively, which are difficult to obtain in practice.

B. Active Power Oscillation Between Parallel VSGs

As depicted in Fig. 2, when the load abruptly changes, the output active power of each VSG will change according to the steady state equation of (1), i.e.,

$$P_{refi} = P^e_{{\rm out}i} + D_i\omega_0\Delta\omega^e_{mi} \tag{2}$$

where the EP of the parallel *N* VSGs system is expressed as

$$\Delta\omega^e_{mi} = \frac{\sum_{i=1}^N P_{refi} - \sum_{i=1}^N P_{{\rm out}i}}{\sum_{i=1}^N D_i\omega_0},$$
$$P^e_{{\rm out}i} = P_{refi} - D_i\omega_0 \cdot \Delta\omega^e_{mi} \tag{3}$$

where $\Delta\omega^e_{mi}$ is the equilibrium value of the difference between ω_{mi} and ω_0, which is identical for parallel VSGs, and $P^e_{{\rm out}i}$ is the equilibrium value of the output active power of the *i*th VSG.

In fact, when the load suddenly changes, the instantaneous active power allocation is determined by the line impedance of VSGs, which can be expressed as

$$\Delta P_1 : \Delta P_2 : \cdots : \Delta P_N = \frac{1/X_1}{\sum_{i=1}^N 1/X_i} : \frac{1/X_2}{\sum_{i=1}^N 1/X_i} : \cdots : \frac{1/X_N}{\sum_{i=1}^N 1/X_i} \tag{4}$$

where ΔP_i $(i = 1, 2, \ldots, N)$ represents the instantaneous change on the output active power of the *i*th VSG caused by the load fluctuation. Based on the analysis above, when the load changes, the EP will be driven to a new point according to (3). If the instantaneous $P_{{\rm out}i}$ after the load change is not equal to the $P^e_{{\rm out}i}$, then the dynamic response of the $P_{{\rm out}i}$ will be induced, which may lead to the active power oscillation. To eliminate the active power oscillation caused by the difference between the instantaneous $P_{{\rm out}i}$ and the $P^e_{{\rm out}i}$, which is needed to be proportional to the capacity of parallel VSGs, the instantaneous change on the active power should satisfy

$$\Delta P_1 : \Delta P_2 : \cdots : \Delta P_N = S_{\rm rate1} : S_{\rm rate2} : \cdots : S_{{\rm rate}N} \tag{5}$$

which can enable the instantaneous $P_{{\rm out}i}$ to be the $P^e_{{\rm out}i}$.

In addition, caused by the change of EP, the ω_{mi} also needs converge to the new equilibrium value $\Delta\omega^e_{mi}$, then the asynchronous response of ω_{mi} will induce interactions between the APL of parallel VSGs. According to [28], induced by the interactions effect above, active power oscillation will not occur only when (5) is satisfied and the parameters J_i and D_i satisfy

$$\frac{J_1}{D_1} = \frac{J_2}{D_2} = \cdots = \frac{J_N}{D_N} \tag{6}$$

which enables synchronization of VSGs when (5) is satisfied.

However, both (5) and (6) are difficult to achieve since the line impedance is uncertain and the free degree of parameter design will be additionally limited, respectively. Therefore, the active power oscillation is further analyzed and addressed in this article.

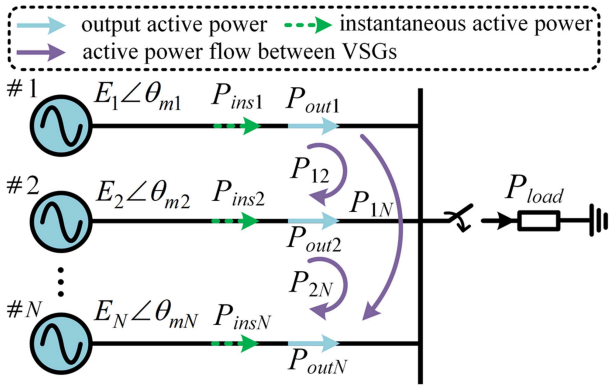

Fig. 3. Active power flow between the parallel VSGs when the load fluctuates.

As depicted in Fig. 3, the active power flow between the parallel VSGs is denoted as P_{ij} ($(j = 1, 2, \ldots, N; j > i)$, which satisfies

$$P_{ji} = -P_{ij}. \tag{7}$$

From (7), it is found that the P_{ij} will not impact the sum of $P_{\mathrm{out}\,i}$, namely

$$\sum_{i=1}^{N} P_{\mathrm{out}i} = P_{\mathrm{load}}. \tag{8}$$

In view of the analysis above, $P_{\mathrm{out}\,i}$ will converge to the $P^e_{\mathrm{out}i}$ as (3) after the load change, i.e., achieving the active power sharing. During this process, the active power flow P_{ij} plays a role in regulating the $P_{\mathrm{out}\,i}$ to its EP $P^e_{\mathrm{out}i}$. From (1), the P_{ij} can be calculated as

$$P_{ij} = \frac{1.5E_iE_j}{X_{ij}} \sin\delta_{ij} = G_{ij}\sin\delta_{ij} \tag{9}$$

where the X_{ij} is equal to $X_i + X_j$, and the δ_{ij} denotes the angle difference between the θ_{mi} and the θ_{mj}.

From (9), the output active power is composed of

$$P_{\mathrm{out}i} = P_{insi} + \sum_{j=1,j\neq i}^{N} P_{ij} = P_{insi} + \sum_{j=1,j\neq i}^{N} G_{ij}\sin\delta_{ij} \tag{10}$$

which indicates the output active power of the ith VSG is composed of the instantaneous power determined by the line impedance, and the active power flow between the parallel VSGs.

And the equilibrium value of the $P_{\mathrm{out}\,i}$ can be expressed as

$$P^e_{\mathrm{out}i} = P_{inis} + \sum_{j=1,j\neq i}^{N} P^e_{ij} = P_{insi} + \sum_{j=1,j\neq i}^{N} G_{ij}\sin\delta^e_{ij} \tag{11}$$

where P_{insi} is the instantaneous active power of the ith VSG after load fluctuation, which is an unknown constant value, P^e_{ij} is the equilibrium value of active power flow between the ith VSG and the jth VSG, and δ^e_{ij} is the equilibrium value of the difference between θ_{mi} and θ_{mj}.

From the analysis abovementioned, impacted by the asynchronous response of ω_{mi} and ω_{mj}, the δ_{ij} will be generated, then it can be found from (10) and (11) that the active power oscillation actually occurs in the active power flow P_{ij}. Differentiating from the single machine grid-connected system, where the power oscillation can be simply analyzed by its transfer function of active power loop, the active power oscillation in parallel VSGs system reflected in P_{ij} (which is related with the coupling effect between parallel VSGs) is much more complex. Thus, in the next section, a parallel VSGs system model is developed to elucidate that the coupling effect is the cause of active power oscillation, and the power oscillation is directly expressed by the time derivative of a Hamiltonian function.

III. Modeling of the Parallel VSGs System

The existing literatures mainly analyze the active power oscillation in terms of transfer function based on small signal modeling, which is sensitive to EP changing induced by the load step and the variation of line impedance. Therefore, in this section, a PCH model of parallel N VSGs system is proposed to prevent the model from being affected by EP changing and investigate coupling effect between parallel VSGs. Moreover, PCH model provides a stable framework for designing control law.

A. Modeling of the Two Parallel VSGs System

As proposed in [31], the PCH theory is widely used in modeling a very large class of physical nonlinear systems in terms of energy dissipation and interconnection. It provides a comprehensive approach to describing the dynamic behavior of these systems based on energy flow. Especially, this theory can be used to describe the energy interconnection between different ports in system network.

To reflect the influence of the active power flow P_{ij} and take the simplicity of the model into account, the two parallel VSGs system is considered as an example and modeled as

$$\begin{cases} \dot{\delta}_{12} = \Delta\omega_{m1} - \Delta\omega_{m2} \\ J_1\omega_0\Delta\dot{\omega}_{m1} = P_{ref1} - (P_{12} + P_{ins1}) - D_1\omega_0\Delta\omega_{m1} \\ J_2\omega_0\Delta\dot{\omega}_{m2} = P_{ref2} - (P_{21} + P_{ins2}) - D_2\omega_0\Delta\omega_{m2} \end{cases} \tag{12}$$

where the active power flow between them is denoted as the P_{12} (-P_{21}), and the instantaneous active power of the 1-th and the 2-th VSG after the load fluctuation are represented as the P_{ins1}, and the $P_{\ ins2}$, respectively.

To analyze the active power oscillation in terms of the PCH system, the (12) needs to be realized as a PCH system as follows:

$$\underbrace{\begin{bmatrix} \dot{\delta}_{12} \\ J_1\omega_0\Delta\dot{\omega}_{m1} \\ J_2\omega_0\Delta\dot{\omega}_{m2} \end{bmatrix}}_{\dot{\boldsymbol{x}}} = \underbrace{\begin{bmatrix} 0 & 1 & -1 \\ -1 & -D_1\omega_0 & 0 \\ 1 & 0 & -D_2\omega_0 \end{bmatrix}}_{J(\boldsymbol{x})-R(\boldsymbol{x})} \underbrace{\begin{bmatrix} G_{12}\sin\delta_{12} \\ \Delta\omega_{m1} \\ \Delta\omega_{m2} \end{bmatrix}}_{\partial H(\boldsymbol{x})/\partial\boldsymbol{x}}$$

$$+\underbrace{\begin{bmatrix}0\\ P_{ref1}-P_{ins,1}\\ P_{ref2}-P_{ins,2}\end{bmatrix}}_{u_0(\boldsymbol{x})} \tag{13}$$

where $\boldsymbol{x}$ denotes the state variables of the PCH system, i.e., $[\delta_{12}, J_1\omega_0\Delta\omega_{m1}, J_2\omega_0\Delta\omega_{m2}]^\top$, $H(\boldsymbol{x})$ is the open loop Hamiltonian function of the PCH system, which represents the energy stored in the PCH system without the impact of input $u_0(\boldsymbol{x})$, and the $J(\boldsymbol{x})$, $R(\boldsymbol{x})$ are the interconnection matrix, dissipation matrix, respectively, which are

$$J(\boldsymbol{x})=\begin{bmatrix}0&1&-1\\-1&0&0\\1&0&0\end{bmatrix}, R(\boldsymbol{x})=\begin{bmatrix}D_1\omega_0&0\\0&D_2\omega_0\end{bmatrix}. \tag{14}$$

From (14), the $J(\boldsymbol{x})$ and the $R(\boldsymbol{x})$ satisfy $J(\boldsymbol{x})=-J^\top(\boldsymbol{x})$ and $R(\boldsymbol{x})=R^\top(\boldsymbol{x})$, which is required by the definition of the PCH system. Additionally, the $u_0(\boldsymbol{x})$ is the original input of the system, which is composed of the reference active power $[P_{ref1}, P_{ref2}]^\top$ and the disturbance $[P_{ins1}, P_{ins2}]^\top$.

Combining (2) and (11), the $[P_{ref1}, P_{ref2}]^\top$ can be divided into

$$\begin{bmatrix}P_{ref1}\\P_{ref2}\end{bmatrix}=\begin{bmatrix}P_{ins1}\\P_{ins2}\end{bmatrix}+\begin{bmatrix}P_{12}^e\\P_{21}^e\end{bmatrix}+\begin{bmatrix}D_1\omega_0\Delta\omega_{m1}^e\\D_2\omega_0\Delta\omega_{m2}^e\end{bmatrix}. \tag{15}$$

Substituting (15) into (13), the instantaneous active power is eliminated, and the PCH system can be modified as

$$\underbrace{\begin{bmatrix}\dot\delta_{12}\\J_1\omega_0\Delta\dot\omega_{m1}\\J_2\omega_0\Delta\dot\omega_{m2}\end{bmatrix}}_{\dot{\boldsymbol{x}}}=\underbrace{\begin{bmatrix}0&1&-1\\-1&-D_1\omega_0&0\\1&0&-D_2\omega_0\end{bmatrix}}_{J(\boldsymbol{x})-R(\boldsymbol{x})}\underbrace{\begin{bmatrix}G_{12}(\sin\delta_{12}-\sin\delta_{12}^e)\\\Delta\omega_{m1}-\Delta\omega_{m1}^e\\\Delta\omega_{m2}-\Delta\omega_{m2}^e\end{bmatrix}}_{\partial H_d(\boldsymbol{x})/\partial\boldsymbol{x}} \tag{16}$$

where the $x^e=[\delta_{12}^e, \Delta\omega_{m1}^e, \Delta\omega_{m2}^e]^\top$ is the EP that enables the $\partial H_d(\boldsymbol{x})/\partial\boldsymbol{x}$ to be 0, and according to (2) and (11), the $\boldsymbol{x}^e$ is the desired EP of the PCH system.

Then, it is found from (16) that the closed loop Hamiltonian function $H_d(\boldsymbol{x})$, which considers the impact of the original input $u_0(\boldsymbol{x})$, can be obtained as

$$H_d(\boldsymbol{x})=\underbrace{\frac{\omega_0}{2}\sum_{k=1}^{2}J_k\Delta\omega_{mk}^2-\omega_0\sum_{k=1}^{2}J_k\Delta\omega_{mk}^e\cdot\Delta\omega_{mk}}_{\text{kinetic energy}}$$
$$\underbrace{-G_{12}\cos\delta_{12}-G_{12}\sin\delta_{12}^e\cdot\delta_{12}}_{\text{potential energy}} \tag{17}$$

where the Hamiltonian function can be decomposed to the kinetic energy and potential energy.

The core of the PCH-based control theory is driving the state variables $\boldsymbol{x}$ to the desired EP rapidly and stably. To represent the location of the state variables $\boldsymbol{x}$, the Hamiltonian function $H_d(\boldsymbol{x})$ is constructed to represent the energy of the PCH system, which should have the minimum value only in the desired EP. The potential energy can be regarded as the difference between the P_{12} and P_{12}^e, which is related with the active power flow between the parallel VSGs, and the kinetic energy represents the difference between $J_k\omega_0\Delta\omega_{mk}$ and $J_k\omega_0\Delta\omega_{mk}^e(k=1,2)$. Furthermore, the dissipation matrix $R(\boldsymbol{x})$ decays the Hamiltonian function $H_d(\boldsymbol{x})$ to make $\boldsymbol{x}$ reach the desired EP as the time increases. Thus, the $H_d(\boldsymbol{x})$ is demanded to be strict minimum in the desired EP, i.e., the $[\delta_{12}^e, \Delta\omega_{m1}^e, \Delta\omega_{m2}^e]^\top$, where the sufficient condition is

$$\begin{cases}\frac{\partial H_d(\boldsymbol{x})}{\partial\boldsymbol{x}}|_{\boldsymbol{x}=\boldsymbol{x}^e}=0\\ Hess(H_d(\boldsymbol{x}))|_{\boldsymbol{x}=\boldsymbol{x}^e}>0\end{cases}. \tag{18}$$

From (16), the $\partial H_d(\boldsymbol{x}^e)/\partial\boldsymbol{x}=0$ is satisfied, and the Hessian matrix of $H_d(\boldsymbol{x})$ in $\boldsymbol{x}^e$ is calculated as

$$Hess(H_d(\boldsymbol{x}))|_{\boldsymbol{x}=\boldsymbol{x}^e}=\begin{bmatrix}G_{12}\cos\delta_{12}^e&0&0\\0&1&0\\0&0&1\end{bmatrix}. \tag{19}$$

Since the δ_{12}^e is within the range of $(-\pi/2, \pi/2)$ in practice, then it can be concluded from (19) that the $Hess(H_d(\boldsymbol{x}^e))>0$, which indicates the $H_d(\boldsymbol{x})$ has a strict minimum in the $\boldsymbol{x}^e$.

B. Modeling of the Parallel N VSGs System

From the last section, the PCH model is built for a two parallel VSGs system. Moreover, the PCH model of the parallel system proposed in this article is promotable and easy to be partitioned. Thus, considering the parallel N VSGs system, as shown in Fig. 2, the PCH model of the parallel N VSGs system is provided as

$$\begin{bmatrix}\dot{\boldsymbol{\delta}}_{\frac{N(N-1)}{2}\times1}\\(J_i\omega_0)_{N\times N}\Delta\dot{\boldsymbol{\omega}}_{N\times1}\end{bmatrix}=\begin{bmatrix}\boldsymbol{0}_{\frac{N(N-1)}{2}\times\frac{N(N-1)}{2}}&(\boldsymbol{J}_{12})_{\frac{N(N-1)}{2}\times N}\\(\boldsymbol{J}_{21})_{N\times\frac{N(N-1)}{2}}&-(\boldsymbol{R}_{22})_{N\times N}\end{bmatrix}\begin{bmatrix}\frac{\partial H_d(\boldsymbol{x})}{\partial\boldsymbol{\delta}}\\\frac{\partial H_d(\boldsymbol{x})}{\partial(J_i\omega_0)_{N\times N}\Delta\boldsymbol{\omega}}\end{bmatrix}. \tag{20}$$

The matrices in (20), the $Hess(H_d(\boldsymbol{x}^e))$ are provided in the Appendix A, and the Hamiltonian function is obtained as

$$H_d(\boldsymbol{x})=E_k+E_p$$
$$\begin{cases}E_k=\frac{\omega_0}{2}\sum_{i=1}^{N}J_i\Delta\omega_{mi}^2-\omega_0\sum_{i=1}^{N}J_i\Delta\omega_{mi}^e\cdot\Delta\omega_{mi}\\E_p=-\sum_{j=1}^{N-1}\sum_{i>j}^{N}G_{ji}\cos\delta_{ji}-\sum_{j=1}^{N-1}\sum_{i>j}^{N}G_{ji}\sin\delta_{ji}^e\cdot\delta_{ji}\end{cases} \tag{21}$$

where E_k and E_p denote the kinetic energy component and the potential energy component, respectively.

It can be found from (21) that the total kinetic energy is composed of the kinetic energy of each VSG, and the total potential energy is related with the active power flow between the parallel VSGs, which implies that the potential energy cannot be exclusively allocated to individual VSGs.

Additionally, the derivative of kinetic energy and potential energy can be used to reflect the direction of energy flows, which

are expressed as

$$\frac{dE_k}{dt} = \left[\frac{\partial H_d(\boldsymbol{x})}{\partial \Delta\boldsymbol{\omega}}\right]^{\top} \boldsymbol{J}_{21} \frac{\partial H_d(\boldsymbol{x})}{\partial \boldsymbol{\delta}} - \left[\frac{\partial H_d(\boldsymbol{x})}{\partial \Delta\boldsymbol{\omega}}\right]^{\top} \boldsymbol{R}_{22} \frac{\partial H_d(\boldsymbol{x})}{\partial \Delta\boldsymbol{\omega}}$$
$$= -\sum_{i=1}^{N}\left[(\Delta\omega_{mi} - \Delta\omega_{mi}^{e}) \cdot \sum_{j\neq i}^{N}(P_{ij} - P_{ij}^{e})\right]$$
$$-\sum_{i=1}^{N} D_i\omega_0(\Delta\omega_{mi} - \Delta\omega_{mi}^{e})^2 \tag{22}$$

$$\frac{dE_p}{dt} = \left[\frac{\partial H_d(\boldsymbol{x})}{\partial \boldsymbol{\delta}}\right]^{\top} \boldsymbol{J}_{12} \frac{\partial H_d(\boldsymbol{x})}{\partial \Delta\boldsymbol{\omega}} = \sum_{i=1}^{N}\left[(\Delta\omega_{mi} - \Delta\omega_{mi}^{e})\right.$$
$$\left.\cdot \sum_{j\neq i}^{N}(P_{ij} - P_{ij}^{e})\right] \tag{23}$$

where the energy flow between the kinetic energy and potential energy is determined by the interconnection matrixes J_{12} and J_{21}, which also represents the coupling effect and the dissipative of energy is determined by the damping matrix R_{22}.

C. Stability of the Parallel N VSGs System

From (21), the derivative of the $H_d(\boldsymbol{x})$ is calculated as

$$\frac{\mathrm{d}H_d(\boldsymbol{x})}{\mathrm{d}t} = -\sum_{i=1}^{N} D_i\omega_0(\Delta\omega_{mi} - \Delta\omega_{mi}^{e})^2 < 0. \tag{24}$$

According to the Laselle invariant principle [29], since the $H_d(\boldsymbol{x})$ is a continuous function, the $\mathrm{d}H_d(\boldsymbol{x})/\mathrm{d}t$ is negative definite (ND), and the desired EP is the only point satisfies that $\partial H_d(\boldsymbol{x})/\partial \boldsymbol{x} = \boldsymbol{0}$, there must exist a constant C such that every state variable starts from the region $\Omega = \{\boldsymbol{x} | \ H_d(\boldsymbol{x}) < \mathrm{C}\}$ will converge to the EP as $t \to \infty$. Thus, the asymptotic stability of the parallel N VSGs system is proved. Moreover, it should be noted that if only the interconnection matrix and the dissipation matrix satisfy the definition of PCH system, the asymptotic stability of the system can always be proven. Compared to the stability analysis of the existing methods, which employs the root locus, or the pole-zero diagram, the stability analysis based on the PCH system is much easier and can be directly generalized to parallel N VSGs system.

D. Impact of the EP Changing

Since the line impedance (which is an equivalent value) of VSG is difficult to obtain in practice and varies with power system network topology changes, the EP of power angle will be impacted by the variation of line impedance. According to the widely used state space matrix of two parallel VSGs system in [28], the dominated poles when the J parameter and the line impedance change are shown in the Fig. 4. It can be found that the poles are not only influenced by control parameters, but also affected by the line impedance, since the line impedance changes the state space matrix of the linearization model.

From Section III-B, the Hamiltonian function has the minimum value in EP, then the state point will converge to its EP as t increases. According to (3), the EP of parallel N VSGs system is dependent on the internal control parameters and the external conditions, i.e., the line impedance and load. Since the EP of power angle in the state space matrix is unavailable even if employs the communication, the parameters in the state space matrix cannot be real time corrected, then the location of eigenvalues is surely influenced by the load changing and different line impedance. The analysis above indicates the robustness of the state space model-based linearization methods will be decreased by EP changing since the eigenvalues are affected. As a comparison, the PCH model and the nonlinear control strategy based on it not rely on regulating locations of eigenvalues and then will not be affected by the EP changing.

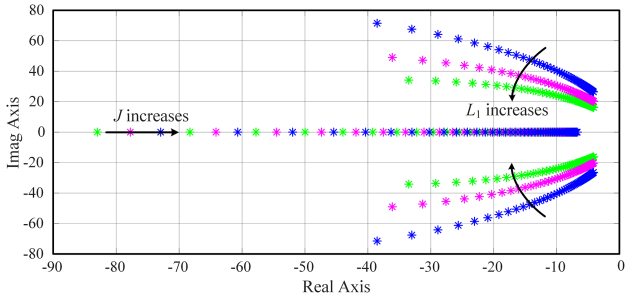

Fig. 4. Dominated poles of the two parallel VSGs system. ($J_2 = 2J_1$, J_1 changes from 0.3 to 20, and L_1 changes from 1 mH to 10 mH while L_2 is always 5 mH.).

E. Mechanism Analysis of the Active Power Oscillation

Equations (20), (22), and (23) demonstrate that the coupling effect (i.e., the J_{12} and J_{21}) determines the energy flow between kinetic energy component and potential energy component of the Hamiltonian function. It can be also found that the Hamiltonian function components are not surely ND owing to the J_{12} and J_{21}, which indicates the coupling effect may causes the oscillation in potential and kinetic energy. However, the impact of coupling effect on the state variables related to each VSG is not investigated. Therefore, this section aims to analyze the mechanism of active power oscillation by quantitatively characterizing the coupling effect between parallel VSGs via its influence on the convergence rate of Hamiltonian function.

From (24), it is found that the $\mathrm{d}H_d(\boldsymbol{x})/\mathrm{d}t$ of the parallel VSGs system is ND, which indicates the total energy of the parallel system will monotonically converge to the EP as $t \to \infty$. However, due to the coupling effect, the convergence rate of the Hamiltonian function related to each state variable cannot be guaranteed to be ND, which are shown as below

$$\frac{\mathrm{d}H_d(J_i\omega_0\Delta\omega_{mi})}{\mathrm{d}t} = \underbrace{-D_i\omega_0(\Delta\omega_{mi} - \Delta\omega_{mi}^{e})^2}_{\text{damping effect}}$$
$$\underbrace{-\sum_{j\neq i}^{N}(P_{ij} - P_{ij}^{e}) \cdot (\Delta\omega_{mi} - \Delta\omega_{mi}^{e})}_{\text{coupling effect}} \tag{25}$$

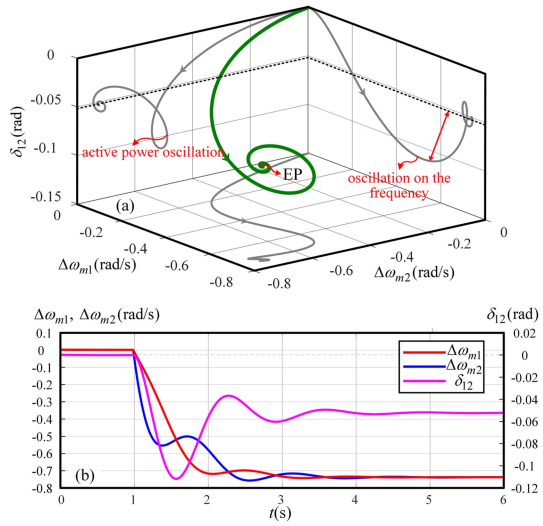

Fig. 5. State variables of the two parallel VSGs system. (a) Trajectories in the state space. (b) Time domain waveforms of the state variables.

$$\frac{\mathrm{d}H_d(\delta_{ij})}{\mathrm{d}t} = \underbrace{(P_{ij} - P_{ij}^e)\cdot(\Delta\omega_{mi} - \Delta\omega_{mj})}_{\text{coupling effect}}. \quad (26)$$

Since the Hamiltonian function of each state variable quantifies its deviation from EP, a positive definite convergence rate implies the oscillatory behavior in that state variable. Impacted by the coupling effect between VSGs, (25) shows that the time derivative of the kinetic energy is difficult to be maintained as ND. Namely, when the coupling effect is larger than the damping effect, the oscillation will occur in angular frequency. And (26) reveals that lack of damping term is likely to induce oscillatory in the active power flow between parallel VSGs, and results in active power oscillation.

Taking the two parallel VSGs system as an example, convergence rate of the Hamiltonian function for each variable are not always ND, which are expressed as

$$\begin{cases} \frac{\mathrm{d}H_d(J_k\omega_0\Delta\omega_{mk})}{\mathrm{d}t} = -D_k\omega_0(\Delta\omega_{mk} - \Delta\omega_{mk}^e)^2 \\ \qquad\qquad -(P_{12} - P_{12}^e)\cdot(\Delta\omega_{mk} - \Delta\omega_{mk}^e) \\ \frac{\mathrm{d}H_d(\delta_{12})}{\mathrm{d}t} = (P_{12} - P_{12}^e)\cdot(\Delta\omega_{m1} - \Delta\omega_{m2}) \end{cases} \quad (27)$$

where the $\mathrm{d}H_d(J_k\omega_0\Delta\omega_{mk})/\mathrm{d}t$ ($k = 12$) and the $\mathrm{d}H_d(\delta_{12})/\mathrm{d}t$ denote the rate of convergence for the state variables $J_k\omega_0\Delta\omega_{mk}$ and δ_{12}.

During the convergence process, only if the convergence rate of state variable remains ND before state variable reaches the EP, the oscillation can be eliminated. However, caused by the coupling effect between the 1-th and 2-th VSG, it is found from (27) that the ND of convergence rate for each state variable cannot be proven. When the δ_{12}-δ_{12}^e has the same symbol as $\Delta\omega_{m1}$-$\Delta\omega_{m2}$, the $\mathrm{d}H_d(\delta_{12})/\mathrm{d}t$ is positive definite, which means the δ_{12} will diverge from the EP, namely, the active power oscillation occurs. Fig. 5 describes the oscillation process comprehensively. As depicted in Fig. 5(a), the δ_{12} exhibits significant oscillation, which indicates the oscillation in active power flow will occur. In addition, the oscillation of the $\Delta\omega_{mk}$ also occurs, which decreases the frequency stability. And it is found in Fig. 5(b) that the oscillation of δ_{12} lasts for seconds, which indicates poor dynamic performance.

From the mechanism analysis above, the active power oscillation is caused by the coupling effect between parallel VSGs, which directly impacts each VSG through the active power flow. Moreover, the impact of coupling effect can be reflected by the energy flow between the kinetic energy and the potential energy. Therefore, in order to mitigate the active power oscillation and enhance the frequency stability, this article proposes a nonlinear strategy based on the L_2-disturbance attenuation control of the PCH model in the following section.

IV. Design of the Proposed Strategy

In this section, based on constraining the impact of coupling effect above, both the mitigation of active power oscillation and the enhancement of frequency stability are achieved by a communication-free control strategy without the need of line impedance and ac bus information.

A. Theoretical Foundations of the Proposed Method

As analyzed in the last section, the coupling effect between parallel VSGs influences each VSG through the active power flow P_{ij}, and the oscillation in both active power and output angular frequency is induced by the coupling effect.

It naturally follows that the mitigation of active power oscillation can be achieved through damping injection in the differential equation of δ_{ij}, namely

$$\dot{\delta}_{ij} = -d_i(P_{ij} - P_{ij}^e) + \Delta\omega_{mi} - \Delta\omega_{mj} \quad (28)$$

where the d_i denotes the damping parameter, and then the (26) is modified to be

$$\frac{\mathrm{d}H_d(\delta_{ij})}{\mathrm{d}t} = \underbrace{-d_i(P_{ij} - P_{ij}^e)^2}_{\text{damping effect}} + (P_{ij} - P_{ij}^e)\cdot(\Delta\omega_{mi} - \Delta\omega_{mj}). \quad (29)$$

From (29), it can be found the damping effect (which is a ND term) is benefit to the convergence of δ_{ij}, which indicates active power oscillation can be mitigated by this damping injection.

However, to support the power system effectively, it is significantly important to remain the inertia of VSG, which implies the general location variable (i.e., δ_{ij}) can only be driven by the general speed variable (i.e., $\Delta\omega_{mi}$-$\Delta\omega_{mj}$). If δ_{ij} is directly driven by the active power flow between the VSGs as (28), then the VSG control will be changed to the conventional droop control, which cannot provide inertia support. Therefore, the active power oscillation cannot be suppressed by injecting damping to the differential equation of δ_{ij} as above.

Fortunately, based on the PCH model above, the impact of coupling effect between parallel VSGs can be reflected by the energy flow between the kinetic energy and the potential energy. Therefore, this article aims to mitigate the oscillation in active power and angular frequency by attenuating the impact of that energy flow. When the energy flow (i.e., the coupling effect) is

constrained, the system achieves both mitigation of active power oscillations and improvement in frequency stability.

As studied in [32], [33], and [34], for the signal belonging to the L_2 space, constraining the impact of this signal can be achieved by the L_2-disturbance attenuation. With a chosen disturbance attenuation level γ, a disturbance signal $\boldsymbol{w}$, and a penalty signal $\boldsymbol{z}$, the achievement of L_2-disturbance attenuation guarantees that

$$\|\boldsymbol{z}\|_2^2 \leq \gamma^2 \|\boldsymbol{w}\|_2^2 . \tag{30}$$

where the $\|\cdot\|$ denotes the two-norm, the penalty signal $\boldsymbol{z}$ is constructed to reflect the deviation of state variables from their desired EPs.

In [32], the PCH system with disturbance is expressed as

$$\begin{cases} \dot{\boldsymbol{x}} = [J(\boldsymbol{x}) - R(\boldsymbol{x})]\frac{\partial H}{\partial \boldsymbol{x}} + g_1(\boldsymbol{x})u(\boldsymbol{x}) + g_2(\boldsymbol{x})\boldsymbol{w} \\ \boldsymbol{z} = h(\boldsymbol{x})[g_1(\boldsymbol{x})]^\top \frac{\partial H}{\partial \boldsymbol{x}} \end{cases} \tag{31}$$

where $g_1(\boldsymbol{x})$ and $g_2(\boldsymbol{x})$ are port structure matrixes, and $h(\boldsymbol{x})$ is the diagonal gain matrix of penalty signal.

Under the condition that

$$R(\boldsymbol{x}) - \frac{1}{2\gamma^2}\left\{g_2(\boldsymbol{x})[g_2(\boldsymbol{x})]^\top - g_1(\boldsymbol{x})[g_1(\boldsymbol{x})]^\top\right\} \geq 0. \tag{32}$$

Inequality (30) can be equivalently expressed as

$$\dot{H}(\boldsymbol{x}) + Q(\boldsymbol{x}) \leq \frac{1}{2}(\gamma^2 \|\boldsymbol{w}\|_2^2 - \|\boldsymbol{z}\|_2^2), Q(\boldsymbol{x}) > 0 \tag{33}$$

which indicates that the change rate of Hamiltonian function is constrained by the penalty signal, and the impact of disturbance on the dynamic response can be constrained. It should be noted that the penalty signal $\boldsymbol{z}$ needs to be designed as a gradient of Hamiltonian function, which can be used to reflect the distance between state variables and their EPs. And a smaller disturbance attenuation level γ indicates better suppression performance against disturbance signals.

Additionally, as studied in [33], the (33) can be achieved by the control law as below

$$u(\boldsymbol{x}) = -\left\{\frac{1}{2}[h(\boldsymbol{x})]^\top h(\boldsymbol{x}) + \frac{1}{2\gamma^2} I\right\}[g_1(\boldsymbol{x})]^\top \frac{\partial H}{\partial \boldsymbol{x}}. \tag{34}$$

B. Proposed Nonlinear Control Strategy

From (3) and (20), it can be found that the gradient field of parallel VSGs is fundamentally indeterminable without communication since the EP requires global information for computation, which will increase system complexity and maintenance costs. Therefore, the penalty signal of this system cannot be directly constructed from the gradient of Hamiltonian function.

To form an obtainable gradient and construct the penalty signal, new state variables are introduced. The control equation of the ith VSG with the introduced state variables is shown as

$$\begin{cases} \dot{\theta}_{mi} = \omega_{mi} + \zeta_i \\ J_i\omega_0\Delta\dot{\omega}_{mi} = P_{refi} - P_{\text{out}i} - D_i\omega_0\Delta\omega_{mi} + D_i\omega_0\zeta_i \\ \dot{\psi}_i = \zeta_i \\ \alpha_i\dot{\zeta}_i = P_{refi} - P_{\text{out}i} - D_i\omega_0\Delta\omega_{mi} - \psi_i \\ z_i = \zeta_i \end{cases} \tag{35}$$

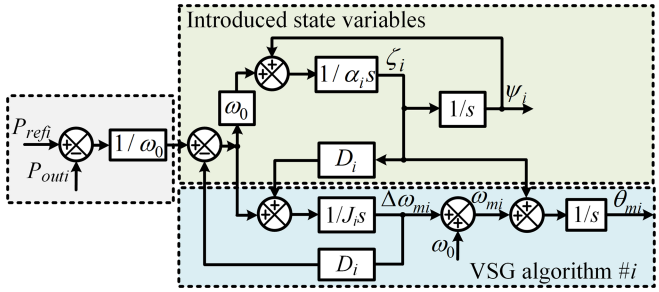

Fig. 6. Control block diagram of the ith VSG with the introduced state variables.

where ψ_i, ζ_i $(i = 1, 2, \ldots, N)$ denote the introduced state variables, α_i represents the control parameters. Furthermore, the parallel VSGs system with introduced state variables are obtained as

$$\begin{bmatrix} \dot{\boldsymbol{\delta}}_{\frac{N(N-1)}{2}\times 1} \\ (J_i\omega_0)_{N\times N}\Delta\boldsymbol{dot\omega}_{N\times 1} \\ \dot{\boldsymbol{\psi}} \\ (\alpha_i)_{N\times N}\dot{\boldsymbol{\zeta}} \end{bmatrix} = \begin{bmatrix} \boldsymbol{0} & \boldsymbol{J}_{12} & \boldsymbol{0} & \boldsymbol{J}_{14} \\ \boldsymbol{J}_{21} & -\boldsymbol{R}_{22} & \boldsymbol{0} & \boldsymbol{J}_{24} \\ \boldsymbol{0} & \boldsymbol{0} & \boldsymbol{0} & \boldsymbol{J}_{34} \\ \boldsymbol{J}_{41} & \boldsymbol{J}_{42} & \boldsymbol{J}_{43} & \boldsymbol{0} \end{bmatrix} \times \begin{bmatrix} \frac{\partial H_c(\boldsymbol{x})}{\partial \boldsymbol{\delta}} \\ \frac{\partial H_c(\boldsymbol{x})}{\partial (J_i\omega_0)_{N\times N}\Delta\boldsymbol{\omega}} \\ \boldsymbol{\psi} \\ \boldsymbol{\zeta} \end{bmatrix} \tag{36}$$

where the $\boldsymbol{J}_{12}, \boldsymbol{J}_{21}, \boldsymbol{R}_{22}$ are identical to that in (20), and the rest matrixes are detailed in Appendix B. Then, it is also proven in Appendix B that the EP of ψ_i and ζ_i are both 0, which indicates the introduced state variables will not affect the EP of output frequency and active power. And the ζ_i will only remain at 0 when the state point of parallel system reaches $\boldsymbol{0}$, implying that the 2-norm of ζ_i will be non-negative and equal 0 if and only if reaches the EP. Furthermore, due to both the EP and state variables are obtainable, partial derivatives of the Hamiltonian with respect to the introduced state variables (i.e., ψ_i, ζ_i) are known. Thus, to constrain the impact of disturbance, penalty signal z_i of the ith VSG is rational to be chosen as ζ_i.

For more intuitive understanding, the control block diagram of parallel VSGs system with the introduced state variables is depicted in Fig. 6. As shown in Fig. 6, the ith VSG contains the original variables and the introduced state variables. Since the derivative of output phase angle θ_{mi} is equal to $\zeta_i + \Delta\omega_{mi}$, the actual output angular frequency of the ith VSG needs to be defined as $\zeta_i + \omega_{mi}$ rather than ω_{mi}.

Since this article focuses on mitigating the oscillation by constraining the impact of coupling effect, the coupling effect between VSGs is treated as the disturbance, and the PCH model with disturbance can be rewritten, as the same form of (31), which has a Hamiltonian function identical to the kinetic energy of (36), and the corresponding matrixes are

$$\boldsymbol{x} = \begin{bmatrix} (J_i\omega_0)_{N\times N}\Delta\boldsymbol{\omega} \\ \boldsymbol{\psi}_{N\times 1} \\ (\alpha_i)_{N\times N}\boldsymbol{\zeta}_{N\times 1} \end{bmatrix}, \frac{\partial H_c}{\partial \boldsymbol{x}}$$

$$= \begin{bmatrix} (\Delta\omega_{mi} - \Delta\omega_{mi}^{e})_{N\times 1} \\ \boldsymbol{\psi}_{N\times 1} \\ \boldsymbol{\zeta}_{N\times 1} \end{bmatrix} \tag{37}$$

$$R(\boldsymbol{x}) = \text{diag}\left[(D_i\omega_0)_{N\times N} \quad \mathbf{0}_{N\times N} \quad \mathbf{0}_{N\times N}\right],$$

$$J(\boldsymbol{x}) = \begin{bmatrix} \mathbf{0}_{N\times N} & \mathbf{0}_{N\times N} & (D_i\omega_0)_{N\times N} \\ \mathbf{0}_{N\times N} & \mathbf{0}_{N\times N} & I_{N\times N} \\ -(D_i\omega_0)_{N\times N} & -I_{N\times N} & \mathbf{0}_{N\times N} \end{bmatrix},$$

$$g_1(\boldsymbol{x}) = \text{diag}\left[\mathbf{0}_{N\times N} \quad I_{N\times N} \quad I_{N\times N}\right] g_2(\boldsymbol{x})$$

$$= \text{diag}\left[I_{N\times N} \quad \mathbf{0}_{N\times N} \quad I_{N\times N}\right]$$

$$\boldsymbol{w} = \text{diag}\left[(P_{\text{out}i} - P_{\text{out}i}^{e})_{N\times 1} \quad \mathbf{0}_{N\times 1} \quad (P_{\text{out}i} - P_{\text{out}i}^{e})_{N\times 1}\right],$$

$$\boldsymbol{z} = \boldsymbol{\zeta}. \tag{38}$$

Then, according to (34), control law of the PCH system above can be calculated as

$$u(\boldsymbol{x}) = \left[(\mathbf{0}_{N\times 1})^{\top} \quad (-(\tfrac{\gamma^2+1}{2\gamma^2})\boldsymbol{\psi}_{N\times 1})^{\top} \quad (-(\tfrac{\gamma^2+1}{2\gamma^2})\boldsymbol{\zeta}_{N\times 1})^{\top}\right] \tag{39}$$

where γ is a constant, which is employed to denote disturbance attenuation level of the PCH system.

C. Design of Control Parameters

New state variables and the L_2-disturbance attenuation introduce some control parameters without tuning. Fortunately, due to the requirement of stability and the interconnection matrix is skew-symmetric, the complexity of parameters design is significantly simplified. Moreover, control parameters of the parallel VSGs system are also constrained by the rate of change of frequency (RoCoF), which is required by the [35].

First, considering the condition as (32), γ needs satisfy that

$$\text{diag}\left[(D_i\omega_0)_{N\times N} \quad \mathbf{0}_{N\times N} \quad \mathbf{0}_{N\times N}\right]$$

$$\geq \frac{\text{diag}\left[I_{N\times N} \quad -I_{N\times N} \quad \mathbf{0}_{N\times N}\right]}{2\gamma^2} \tag{40}$$

which leads to

$$\gamma_{\min} \geq \max\left(\frac{1}{\sqrt{2D_i\omega_0}}\right), i = 1, 2, \ldots, N. \tag{41}$$

Since the parameter γ denotes the disturbance attenuation level, a smaller value of γ indicates superior disturbance attenuation effect, the γ should be designed as a smallest achievable value constrained by (41).

Then, control parameters of the introduced state variables are shown as below. In [35], the transient RoCoF is required to be smaller than 3 Hz/s. Assuming the peak transient power output reaches 2 times the rated capacity (i.e., $3P_{refi}$), thus, according to (36) and the initial value theorem, α_i of the ith VSG is constrained by

$$\left(\frac{1}{J_i\omega_0} + \frac{1}{\alpha_i}\right) \leq \frac{3\pi}{P_{refi}}. \tag{42}$$

Furthermore, based on the time-scale decoupling theory, the α_i cannot be much larger than the $J_i\omega_0$, which makes the ζ_i a "slow variable" and then slows down the dynamic process. Thus, considering the constraint of (42) and a rapid dynamic response, the α_i is designed to be

$$\alpha_i \geq \frac{P_{refi}J_i\omega_0}{3\pi J_i\omega_0 - P_{refi}}. \tag{43}$$

Compared with the parameters design of conventional methods through bode diagram and root locus, which are susceptible to EP changes, parameters of proposed strategy are only related with the rated capacity, damping, and inertia parameters. Therefore, the proposed strategy demonstrates superior robustness, which is verified in Section V-A.

To make the implementation of the proposed control strategy intuitive, the schematic diagram of the proposed strategy in the parallel N VSGs system are depicted as Fig. 7, where the control block diagram of the ith VSG is taken as an example for detailed illustration.

In Fig. 7, the disturbance attenuation level γ can be designed in advance, and the α_i can be designed according to P_{refi} and J_i of the ith VSG. Moreover, the control law of the ith VSG is only related with ψ_i, ζ_i, which can be obtained locally. Therefore, the proposed strategy is communication-free, which reduces the system complexity.

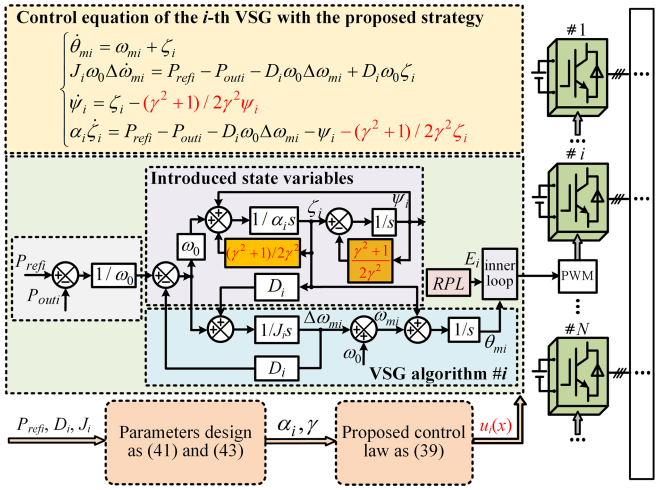

Fig. 7. Schematic diagram of parallel VSGs system with the proposed strategy.

D. Stability of the Parallel VSGs System With the Proposed Strategy

The proof is provided in Appendix C.

V. Simulations and Experiments

To demonstrate the proposed strategy, a system made up of two parallel VSGs is established, the simulations based on

TABLE I
PARAMETERS OF EXPERIMENTS AND SIMULATIONS

symbol	value	symbol	value
U_{dck} (k=1,2)	700 V	J_1, J_2	2.5, 5
U_{refk}	220 V (RMS)	L_1, L_2	5 mH, 10 mH
S_{ratek}	5 kVA (1 p.u.)	R_k	0.5 Ω
ω_0	100π rad/s	L_{fk}	5 mH
D_k	4 (sim.)/6 (exp.)	C_{fk}	9.4 μF
α_1, α_2	1500, 800	γ	0.025 (sim.) 0.02(exp.)

the MATLAB/Simulink and the experiments that employ the hardware platform are carried out. Main parameters are shown in Table I. The inductance is chosen as a large value to maintain the transmission line to be an inductive line.

A. Simulation Results

This section aims at validating the effectiveness of the proposed strategy on mitigating active power oscillation and enhancing the frequency stability. It should be noted that output angular frequency of the VSG with the proposed strategy is replaced by $\zeta_i+\omega_{mi}$ (which is represented by ω_i) since phase angle of VSG is actually determined by $\zeta_i+\omega_{mi}$ rather than ω_{mi}.

In Fig. 8, the output active power and the angular frequency waveforms of the two parallel VSGs system are provided.

As shown in Fig. 8(a), VSGs without the proposed method are employed. When the load step occurs, the instantaneous change on active power is determined by the line impedance as (4), which cannot be regulated by control methods. Then, the active power of VSG will converge to the desired EP, it can be found the active power oscillation is severe, and oscillation in frequency indicates the frequency stability of parallel system is damaged by active power oscillation.

As shown in Fig. 8(b), VSGs with the proposed strategy are employed, where the disturbance attenuation level γ is much larger than the minimum value of γ constrained by (41), which indicates the capability on mitigating oscillation is not fully utilized. As a result, although the active power oscillation is mitigated, and the frequency stability is also enhanced, since the disturbance attenuation level is relatively higher (lower disturbance attenuation level means better performance), oscillation in active power and angular frequency cannot be mitigated effectively.

As shown in Fig. 8(c), VSGs with the proposed strategy are employed in parallel system and the γ is 0.025, which is the smallest value constrained by (41). When the load step occurs, the instantaneous active power of VSG is determined by the line impedance as (4). Then, the active power flow between the VSGs is generated by the asynchronous frequency and achieves the active power sharing. During this process, benefitting from the proposed strategy, it is found that the active power oscillation is eliminated and the frequency stability is improved, which exhibits better control performance than the proposed strategy with $\gamma = 0.5$. Although transient RoCoF as the load changes is larger than that of traditional VSGs parallel system, constrained by the (43), RoCoF satisfies the requirement of [35]. Moreover, differentiating from the methods proposed in [24], [26], [27], [28], and [30], where the inertia is eliminated or the RoCoF is lack of constraint, the RoCoF of VSG with the proposed strategy satisfies the requirement of [35].

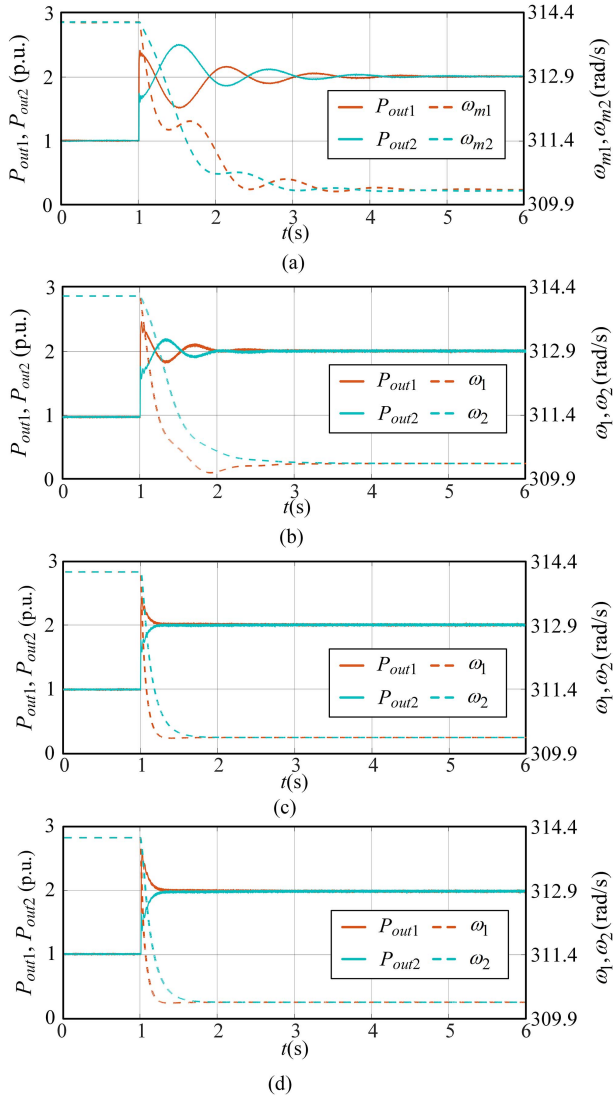

Fig. 8. Simulation results of the two parallel VSGs system when the load changes from 1.0 p.u. to 2.0 p.u. (a) Traditional VSGs. (b) VSGs with the proposed strategy when the γ is 0.5. (c) VSGs with the proposed strategy when the γ is 0.025. (d) VSGs with the proposed strategy when the γ is 0.025, and the $L_1 = 4$ mH, $L_2 = 12$ mH.

Furthermore, to demonstrate the robustness of the proposed strategy as the line impedance changes (i.e., the EP changing), the L_1, L_2 are changed to be 4 mH, 12 mH, respectively. Then, instantaneous difference between active power and its EP is increased as (4), and the EP of power angle is changed, which will impact the share of instantaneous active power and the location of eigenvalues for linear model. However, as shown in Fig. 8(d), it can be observed that the effectiveness of the proposed strategy is not influenced, which proves the robustness of the proposed strategy when the EP changes.

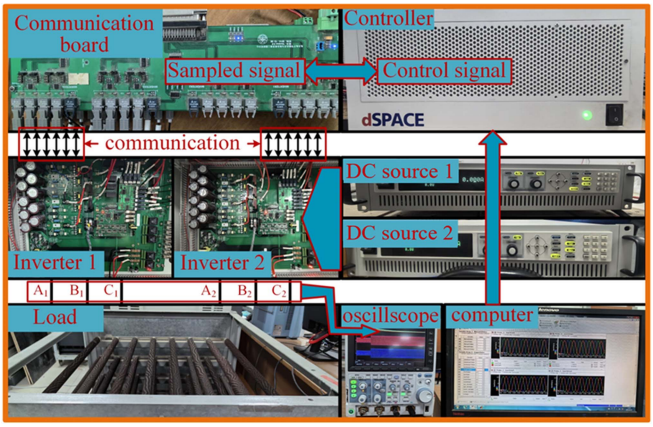

Fig. 9. Experimental system.

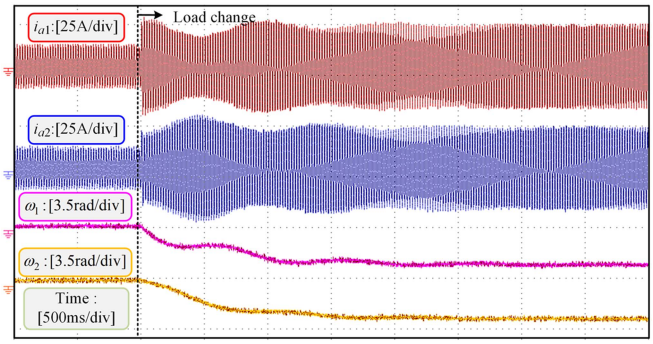

Fig. 10. Experiment results of the two parallel VSGs system without any strategy when the load changes from 1.0 p.u. to 2.0 p.u.

B. Experiment Results

To verify the effectiveness of the proposed strategy, the comparative experiment was conducted, and the corresponding experiment platform is shown in Fig. 9, which was composed of two parallel inverters and an adjustable load. Moreover, the main circuit of experiment platform is shown as the Figs. 1 and 2. The proposed strategy was implemented by dSPACE platform, and a 4-channel oscilloscope was used to capture the output waveform, where the output frequency and active power were obtained by a digital-analog converter (DAC) module. Parameters of experiment are shown in the Table I. To avoid all the results being generated by the DAC module of dSPACE platform, the output current of VSGs, which were directly measured by the current clamp were used to replace the active power in simulation results. Moreover, since the change on ω_{mi} is much smaller than the nominal value of ω_{mi}, which is easy to be impacted by the noise signal of hardware, $\Delta\omega_{mi}$ is employed to show the dynamic response of output frequency.

In Fig. 10, when the load change occurs, the instantaneous active power is shared as (4), which is only determined by the line impedance. Then, during the convergence process of active powers to their EP values, it can be found that even if the damping D_i is larger than that of simulation, the active power oscillation occurs when the load changes, and the frequency stability is also not guaranteed.

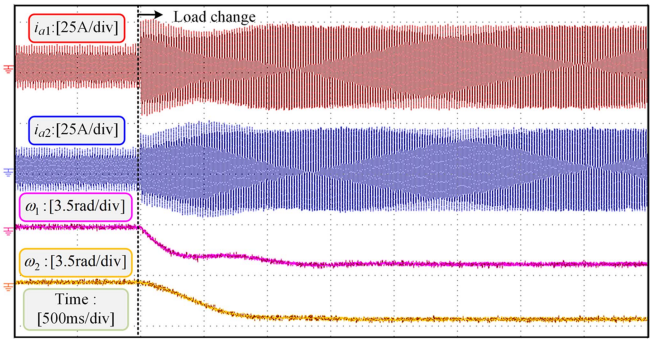

Fig. 11. Experiment results of the two parallel VSGs system with the proposed strategy when the $\gamma = 0.5$.

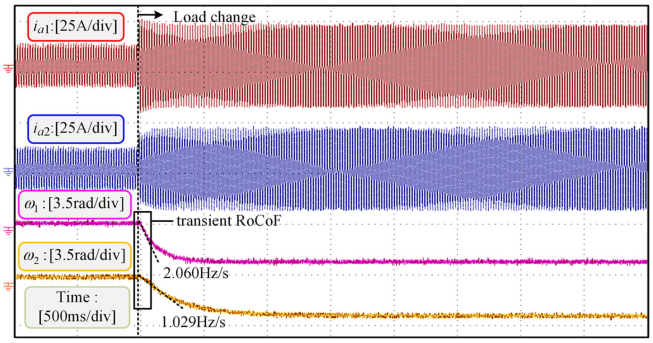

Fig. 12. Experiment results of the two parallel VSGs system with the proposed strategy when the $\gamma = 0.02$.

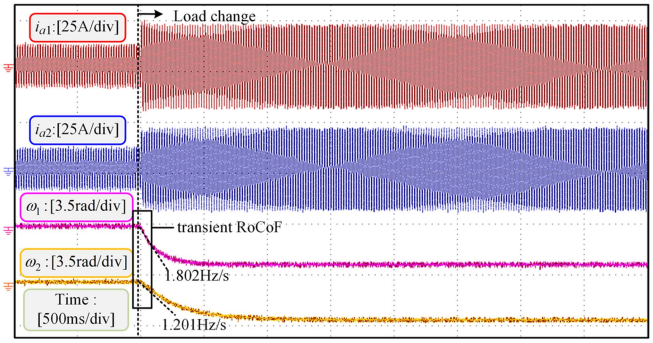

Fig. 13. Experiment results of the two parallel VSGs system with the proposed strategy when the $\gamma = 0.02$ and the line impedance L_1, L_2 are changed to be 4 mH, 6 mH, repectively.

In Fig. 11, the proposed strategy with the $\gamma = 0.5$ is employed, which means the disturbance attenuation level is much larger than the limitation value constrained by (41). When the load change occurs, it can be found that the active power oscillation is partly mitigated. However, the effectiveness of this method is limited, the improvement on active power and angular frequency is nonremarkable.

In Fig. 12, the proposed strategy with the $\gamma = 0.02$ is employed, which is a minimally achievable value constrained by (41). When the load abruptly changes, the instantaneous active power of parallel VSGs will be shared as (4). Then, during the process of active power sharing, it can be found that the active power oscillation is mitigated effectively, and the angular frequency converges to its EP smoothly, which indicates that the frequency stability is enhanced. Although the transient RoCoF of the parallel VSGs system with the proposed strategy as the load changes is larger than that of the parallel VSGs system without control, the RoCoF can still satisfies the requirement of [35] by designing the α_i as (43). Compared to the result of Fig. 11, the proposed with the $\gamma = 0.02$ more effectively mitigates the active power oscillation, which agrees with the theoretical analysis that the smaller disturbance level implies the better constraint on the impact of disturbance, i.e., the coupling effect between parallel VSGs.

In Fig. 13, the proposed strategy with the $\gamma = 0.02$ is employed and the line impedance are changed to $L_1 = 4$ mH, $L_2 = 6$ mH, respectively. According to (4), the reduced impedance mismatch between parallel VSGs makes the instantaneous active power deviation diminished when the load abruptly changes. It can be found from Fig. 13 that the active power oscillation is mitigated effectively and the frequency stability is enhanced, which furthermore verifies the robustness of the proposed strategy as the line impedance varies.

From the analysis above, it can be found that the experimental results are consistent with the simulation results. Moreover, both the simulation results and the experiment results agree with the theoretical analysis that the effective mitigation of active power and the frequency stability can be guaranteed by the proposed strategy at the same time.

VI. Conclusion

This article addresses the active power oscillation and enhances the frequency stability in the parallel VSGs system. The PCH model of this system is first built in terms of the active power flow between the parallel VSGs, which provides a stable framework for designing control law and improves the robustness of the proposed strategy based on it. Then, based on the PCH model, impact of the coupling effect between parallel VSGs are researched. Furthermore, the coupling effect is regarded as the disturbance, and its impact is constrained by the proposed communication-free nonlinear control strategy based on the L_2-disturbance attenuation, which is employed to mitigate the active power oscillation and enhance the frequency stability. Finally, effectiveness of the proposed strategy is verified by the simulation and experiment.

Appendix

Appendix A

The matrices in (20) are

$$\boldsymbol{\delta} = [\underbrace{\delta_{12}\cdots\delta_{1N}}_{N-1}\underbrace{\delta_{23}\cdots\delta_{2N}}_{N-2}\cdots\delta_{N-1,N}], \Delta\boldsymbol{\omega} = [\underbrace{J_1\omega_0\Delta\omega_{m1}J_2\omega_0\Delta\omega_{m2}\cdots J_N\omega_0\Delta\omega_{mN}}_{N}] \tag{44}$$

$$\boldsymbol{R}_{22} = diag(\underbrace{-D_1\omega_0\Delta\omega_{m1} \quad -D_2\omega_0\Delta\omega_{m2} \quad \cdots \quad -D_N\omega_0\Delta\omega_{mN}}_{N}), \boldsymbol{J}_{21} = \underbrace{\begin{bmatrix} -1 & \cdots & -1 & 0 & \cdots & 0 & \cdots & 0 \\ 1 & \mathbf{0} & 0 & -1 & \cdots & -1 & \ldots & 0 \\ \mathbf{0} & \ddots & \mathbf{0} & 1 & \mathbf{0} & 0 & \cdots & \vdots \\ 0 & \mathbf{0} & 1 & \mathbf{0} & \ddots & \mathbf{0} & \cdots & 0 \\ 0 & \mathbf{0} & 0 & 0 & \mathbf{0} & 1 & \cdots & -1 \\ 0 & \mathbf{0} & 0 & 0 & \mathbf{0} & 0 & \cdots & 1 \end{bmatrix}}_{N\times\frac{N(N-1)}{2}},$$

$$\boldsymbol{J}_{12} = -\boldsymbol{J}_{21}^{\top} \tag{45}$$

$$\frac{\partial H_d(\boldsymbol{x})}{\partial\boldsymbol{\delta}} = [G_{12}(\sin\delta_{12} - \sin\delta_{12}^e) \quad \cdots \quad G_{1N}(\sin\delta_{1N} - \sin\delta_{1N}^e) \quad G_{23}(\sin\delta_{23} - \sin\delta_{23}^e) \quad \cdots \quad G_{2N}(\sin\delta_{2N} - \sin\delta_{2N}^e)$$

$$\cdots \quad G_{N-1,N}(\sin\delta_{N-1,N} - \sin\delta_{N-1,N}^e)]^{\top}$$

$$\frac{\partial H_d(\boldsymbol{x})}{\partial\Delta\boldsymbol{\omega}} = [\Delta\omega_{m1} - \Delta\omega_{m1}^e\Delta\omega_{m2} - \Delta\omega_{m2}^e\cdots\Delta\omega_{mN} - \Delta\omega_{mN}^e]^{\top} \tag{46}$$

$$Hess(H_d(\boldsymbol{x}))|_{\boldsymbol{x}=\boldsymbol{x}^e} = \begin{bmatrix} G_{12}\cos\delta_{12}^e & \mathbf{0} & 0 \\ \mathbf{0} & \ddots & \mathbf{0} \\ 0 & \mathbf{0} & G_{N-1,N}\cos\delta_{N-1,N}^e \end{bmatrix}. \tag{47}$$

Appendix B

The rest matrixes in (36) are

$$\begin{aligned}&\boldsymbol{J}_{14}=I_{N\times N},\boldsymbol{J}_{24}=(D_i\omega_0)_{N\times N},\boldsymbol{J}_{34}=I_{N\times N}\\&\boldsymbol{J}_{14}=-(\boldsymbol{J}_{41})^{\top},\boldsymbol{J}_{24}=-(\boldsymbol{J}_{42})^{\top},\boldsymbol{J}_{34}=-(\boldsymbol{J}_{43})^{\top}.\end{aligned}\tag{48}$$

And the Hamiltonian function is

$$\begin{aligned}H_c(x)=&\frac{\omega_0}{2}\sum_{i=1}^{N}J_i\Delta\omega_{mi}^2-\omega_0\sum_{i=1}^{N}J_i\Delta\omega_{mi}^e\cdot\Delta\omega_{mi}\\&-\sum_{j=1}^{N-1}\sum_{i>j}^{N}G_{ji}\cos\delta_{ji}-\sum_{j=1}^{N-1}\sum_{i>j}^{N}G_{ji}\sin\delta_{ji}^e\cdot\delta_{ji}\\&+\frac{1}{2}\sum_{i=1}^{N}\psi_i^2+\frac{1}{2}\sum_{i=1}^{N}\alpha_i\zeta_i^2\end{aligned}\tag{49}$$

where the $H_c(\boldsymbol{x})$ is equal to the sum of $H_d(\boldsymbol{x})$ and the quadratic form of ψ_i and ζ_i.

Appendix C

With the proposed control law, the closed loop form of (36) can be obtained as

$$\begin{aligned}&\begin{bmatrix}\dot{\boldsymbol{\delta}}_{\frac{N(N-1)}{2}\times1}\\(J_i\omega_0)_{N\times N}\Delta\dot{\boldsymbol{\omega}}_{N\times1}\\\dot{\boldsymbol{\psi}}\\(\alpha_i)_{N\times N}\dot{\boldsymbol{\zeta}}\end{bmatrix}=\begin{bmatrix}\boldsymbol{0}&\boldsymbol{J}_{12}&\boldsymbol{0}&\boldsymbol{J}_{14}\\\boldsymbol{J}_{21}&-\boldsymbol{R}_{22}&\boldsymbol{0}&\boldsymbol{J}_{24}\\\boldsymbol{0}&\boldsymbol{0}&\boldsymbol{0}&\boldsymbol{J}_{34}\\\boldsymbol{J}_{41}&\boldsymbol{J}_{42}&\boldsymbol{J}_{43}&\boldsymbol{0}\end{bmatrix}\\&\quad\times\begin{bmatrix}\frac{\partial H_c(\boldsymbol{x})}{\partial\boldsymbol{\delta}}\\\frac{\partial H_c(\boldsymbol{x})}{\partial\Delta\boldsymbol{\omega}}\\\boldsymbol{\psi}\\\boldsymbol{\zeta}\end{bmatrix}+g_1(\boldsymbol{x})u(\boldsymbol{x})\\&=\begin{bmatrix}\boldsymbol{0}&I_{N\times N}&\boldsymbol{0}&I_{N\times N}\\-I_{N\times N}&-(D_i\omega_0)_{N\times N}&\boldsymbol{0}&(D_i\omega_0)_{N\times N}\\\boldsymbol{0}&\boldsymbol{0}&-\frac{\gamma^2+1}{2\gamma^2}I_{N\times N}&I_{N\times N}\\-I_{N\times N}&-(D_i\omega_0)_{N\times N}&-I_{N\times N}&-\frac{\gamma^2+1}{2\gamma^2}I_{N\times N}\end{bmatrix}\\&\quad\times\begin{bmatrix}\frac{\partial H_c(\boldsymbol{x})}{\partial\boldsymbol{\delta}}\\\frac{\partial H_c(\boldsymbol{x})}{\partial\Delta\boldsymbol{\omega}}\\\boldsymbol{\psi}\\\boldsymbol{\zeta}\end{bmatrix}\end{aligned}\tag{50}$$

and the closed loop Hamiltonian function is same as that in (49).

Furthermore, from (18) and (50), it can be found the EP of δ_{ij} and $\Delta\omega_{mi}$ are identical to that of (20), and the EP of ψ_i, ζ_i are 0. Since the closed loop system still satisfies the requirement of interconnection matrix and dissipative matrix, stability of the closed loop system can be proven as that in Section III-C and the state point will converge to the desired EP as $t\to\infty$.

REFERENCES

[1] R. H. Lasseter, "MicroGrids," in *Proc. IEEE Power Eng. Soc. Winter Meeting*, 2002, pp. 305–308.

[2] J. Rocabert, A. Luna, F. Blaabjerg, and P. Rodríguez, "Control of power converters in AC microgrids," *IEEE Trans. Power Electron.*, vol. 27, no. 11, pp. 4734–4749, Nov. 2012.

[3] A. Karimi et al., "Inertia response improvement in AC microgrids: A fuzzy-based virtual synchronous generator control," *IEEE Trans. Power Electron.*, vol. 35, no. 4, pp. 4321–4331, Apr. 2020.

[4] C. Li et al., "New framework of RoCoF-FD for wideband stability evaluation in renewable energy generators with virtual impedance control," *IEEE Trans. Smart Grid*, vol. 13, no. 5, pp. 3570–3581, Sep. 2022.

[5] W. Wu et al., "Sequence-impedance-based stability comparison between VSGs and traditional grid-connected inverters," *IEEE Trans. Power Electron.*, vol. 34, no. 1, pp. 46–52, Jan. 2019.

[6] G. Li et al., "Analysis and mitigation of subsynchronous resonance in series-compensated grid-connected system controlled by a virtual synchronous generator," *IEEE Trans. Power Electron.*, vol. 35, no. 10, pp. 11096–11107, Oct. 2020.

[7] H. Wu et al., "Small-signal modeling and parameters design for virtual synchronous generators," *IEEE Trans. Ind. Electron.*, vol. 63, no. 7, pp. 4292–4303, Jul. 2016.

[8] Q. Zhang, D. Zheng, and P. Zhang, "A review of junction temperature monitoring and control methods for SiC MOSFETs," in *Proc. CSEE*, 2025, pp. 1–18, doi: 10.13334/j.0258-8013.pcsee.241303.

[9] J. M. Guerrero, L. G. de Vicuna, J. Matas, M. Castilla, and J. Miret, "Output impedance design of parallel-connected UPS inverters with wireless load-sharing control," *IEEE Trans. Ind. Electron.*, vol. 52, no. 4, pp. 1126–1135, Aug. 2005.

[10] T. Wu, Z. Liu, J. Liu, S. Wang, and Z. You, "A unified virtual power decoupling method for droop-controlled parallel inverters in microgrids," *IEEE Trans. Power Electron.*, vol. 31, no. 8, pp. 5587–5603, Aug. 2016.

[11] J. Chen and T. O'Donnell, "Parameter constraints for virtual synchronous generator considering stability," *IEEE Trans. Power Syst.*, vol. 34, no. 3, pp. 2479–2481, May 2019.

[12] X. Meng, J. Liu, and Z. Liu, "A generalized droop control for grid-supporting inverter based on comparison between traditional droop control and virtual synchronous generator control," *IEEE Trans. Power Electron.*, vol. 34, no. 6, pp. 5416–5438, Jun. 2019.

[13] J. Alipoor, Y. Miura, and T. Ise, "Power system stabilization using virtual synchronous generator with alternating moment of inertia," *IEEE J. Emerg. Sel. Topics Power Electron.*, vol. 3, no. 2, pp. 451–458, Jun. 2015.

[14] A. Jain, M. K. Pathak, and N. P. Padhy, "Conjoint enhancement of VSG dynamic output responses by disturbance-oriented adaptive parameters," *IEEE Trans. Ind. Inform.*, vol. 20, no. 2, pp. 2079–2096, Feb. 2024.

[15] Y. Chen, B. Zhang, D. Qiu, Y. Chen, F. Xie, and H. Sun, "Switched active power control of a grid-connected inverter with reduced RoCoF and frequency overshoot," *IEEE Trans. Power Electron.*, vol. 39, no. 4, pp. 4062–4077, Apr. 2024.

[16] M. Yang, Y. Wang, X. Xiao, and Y. Li, "A robust damping control for virtual synchronous generators based on energy reshaping," *IEEE Trans. Energy Convers.*, vol. 38, no. 3, pp. 2146–2159, Sep. 2023.

[17] G. W. Chang and K. T. Nguyen, "A new adaptive inertia-based virtual synchronous generator with even inverter output power sharing in islanded microgrid," *IEEE Trans. Ind. Electron.*, vol. 71, no. 9, pp. 10693–10703, Sep. 2024, doi: 10.1109/TIE.2023.3327515.

[18] H. Xu, C. Yu, C. Liu, Q. Wang, F. Liu, and F. Li, "An improved virtual capacitor algorithm for reactive power sharing in multi-paralleled distributed generators," *IEEE Trans. Power Electron.*, vol. 34, no. 11, pp. 10786–10795, Nov. 2019.

[19] J. Liu, Y. Miura, H. Bevrani, and T. Ise, "Enhanced virtual synchronous generator control for parallel inverters in microgrids," *IEEE Trans. Smart Grid*, vol. 8, no. 5, pp. 2268–2277, Sep. 2017.

[20] Z. Shuai, W. Huang, Z. J. Shen, A. Luo, and Z. Tian, "Active power oscillation and suppression techniques between two parallel synchronverters during load fluctuations," *IEEE Trans. Power Electron.*, vol. 35, no. 4, pp. 4127–4142, Apr. 2020.

[21] S. Chen, Y. Sun, H. Han, G. Shi, Y. Guan, and J. M. Guerrero, "Dynamic frequency performance analysis and improvement for parallel VSG systems considering virtual inertia and damping coefficient," *IEEE J. Emerg. Sel. Topics Power Electron.*, vol. 11, no. 1, pp. 478–489, Feb. 2023.

[22] Y. Yu, S. K. Chaudhary, G. D. A. Tinajero, L. Xu, J. C. Vasquez, and J. M. Guerrero, "Active damping for dynamic improvement of multiple grid-tied virtual synchronous generators," *IEEE Trans Ind. Electron.*, vol. 71, no. 4, pp. 3673–3683, Apr. 2024.

[23] A. González-Cajigas, J. Roldán-Pérez, and E. J. Bueno, "Design and analysis of parallel-connected grid-forming virtual synchronous machines for island and grid-connected applications," *IEEE Trans. Power Electron.*, vol. 37, no. 5, pp. 5107–5121, May 2022,.

[24] M. Li et al., "Phase feedforward damping control method for virtual synchronous generators," *IEEE Trans. Power Electron.*, vol. 37, no. 8, pp. 9790–9806, Aug. 2022.

[25] M. Chen, D. Zhou, C. Wu, and F. Blaabjerg, "Characteristics of parallel inverters applying virtual synchronous generator control," *IEEE Trans. Smart Grid*, vol. 12, no. 6, pp. 4690–4701, Nov. 2021.
[26] L. Li, Y. Sun, M. Su, and S. Fu, "Decentralized mutual damping control of cascaded-type VSGs for power and frequency oscillation suppression," *IEEE Trans. Ind. Electron.*, vol. 69, no. 10, pp. 10215–10226, Oct. 2022.
[27] Z. Wang et al., "Active power oscillation suppression based on decentralized transient damping control for parallel virtual synchronous generators," *IEEE Trans. Smart Grid*, vol. 14, no. 4, pp. 2582–2592, Jul. 2023.
[28] M. Chen, D. Zhou, and F. Blaabjerg, "Active power oscillation damping based on acceleration control in paralleled virtual synchronous generators system," *IEEE Trans. Power Electron.*, vol. 36, no. 8, pp. 9501–9510, Aug. 2021.
[29] N. G. Bretas and L. F. C. Alberto, "Lyapunov function for power systems with transfer conductances: Extension of the invariance principle," *IEEE Trans. Power Sys.*, vol. 18, no. 2, pp. 769–777, May 2003.
[30] B. Yang, H. Li, S. Xu, H. Liu, and S. Lu, "Systematic methods to eliminate the transient circulating powers in the Multi-VSGs system," *IEEE Trans. Smart Grid*, vol. 15, no. 1, pp. 179–190, Jan. 2024.
[31] R. Ortega et al., "Interconnection and damping assignment passivity-based control of port-controlled Hamiltonian systems," *Automatica*, vol. 38, no. 4, pp. 585–596, Apr. 2002.
[32] V. Schaft, *L2-Gain and Passivity Techniques in Nonlinear Control*. Berlin, Germany: Springer, 1999.
[33] Y. Wang, D. Cheng, C. Li, and Y. Ge, "Dissipative Hamiltonian realization and energy-based L_2-disturbance attenuation control of multimachine power systems," *IEEE Trans. Automat. Control*, vol. 48, no. 8, pp. 1428–1433, Aug. 2003.
[34] Y. Wang, G. Feng, D. Cheng, and Y. Liu, "Adaptive L_2 disturbance attenuation control of multi-machine power systems with SMES units," *Automatica*, vol. 42, no. 7, pp. 1121–1132, Jul. 2006.
[35] *IEEE standard for interconnection and interoperability of distributed energy resources with associated electric power systems interfaces*, IEEE Standard 1547.2-2023, May 2024.

Jiadong Sun was born in Weifang, China, in 2000. He received the B.S. degree in electrical engineering from Qingdao University, Qingdao, China, in 2022. He is currently working toward the Ph.D. degree in power electronics and power transmission with the School of Control Science and Engineering, Shandong University, Jinan, China.

His research interests include the stability analysis and control strategy of renewable energy power generation system.

Xiangyang Xing (Member, IEEE) was born in Rizhao, China, in 1985. He received the B.S. degree in automation and the M.S. degree in control theory and application from Qufu Normal University, Qufu, China, in 2009 and 2012, respectively, and the Ph.D. degree in electrical engineering from Shandong University, Jinan, China, in 2016

From 2017 to 2019, he was a Postdoctoral Research Fellow with Shandong University. In 2019, he was with Shandong University, where he is currently a Full Professor with the School of Control Science and Engineering. His research interests include multilevel converters, power conversion, and renewable power generation.

Chenghui Zhang (Fellow, IEEE) received the B.S. and M.S. degrees in automation engineering from Shandong University of Technology, Jinan, China, in 1985 and 1988, respectively, and the Ph.D. degree in control theory and operational research from Shandong University, Jinan, China, in 2001.

In 1988, he was with Shandong University, where he is currently a Professor with the School of Control Science and Engineering. He is also the Chief Manager of Power Electronic Energy-Saving Technology and Equipment Research Center of Education Ministry, Jinan, China. His research interests include optimal control of engineering, power electronics and motor drives, energy-saving techniques, and time-delay systems.